Anomalous dispersion with excitation wavelength of longitudinal optical phonon–plasmon coupled modes in n-InGaAs

2004 J. Phys.: Condens. Matter 16 971

(http://iopscience.iop.org/0953-8984/16/6/024)

INSTITUTE OF PHYSICS PUBLISHING JOURNAL OF PHYSICS: CONDENSED MATTER

J. Phys.: Condens. Matter **16** (2004) 971–978 PII: S0953-8984(04)70877-2

Anomalous dispersion with excitation wavelength of longitudinal optical phonon–plasmon coupled modes in n-InGaAs

S Hernández[1], R Cuscó[1], J Ibáñez[1], M Hopkinson[2] and L Artús[1]

[1] Institut Jaume Almera, Consell Superior d'Investigacions Científiques (CSIC), Lluís Solé i Sabarís sn, 08028 Barcelona, Spain
[2] Department of Electronics and Electrical Engineering, University of Sheffield, Sheffield S1 3JD, UK

Received 21 October 2003
Published 30 January 2004
Online at stacks.iop.org/JPhysCM/16/971 (DOI: 10.1088/0953-8984/16/6/024)

Abstract

We have studied the wavevector dispersion of the L_+ coupled mode in n-type $In_{0.53}Ga_{0.47}As$ by means of Raman scattering using several excitation wavelengths in the range between 457.9 and 720 nm. The optical properties of $In_{0.53}Ga_{0.47}As$ in the range of excitation energies used are strongly affected by the presence of the E_1 and $E_1 + \Delta_1$ critical points, and set an upper limit to the wavevector that can be probed by decreasing the excitation wavelength in Raman scattering experiments. The Raman scattering results are analysed using a Lindhard–Mermin model, and it is found that optical absorption strongly affects the coupled-mode Raman peaks excited with the more energetic lines.

1. Introduction

In doped polar semiconductors, free carriers interact with the longitudinal optical (LO) phonons via their macroscopic electric field and, as a consequence, coupling between them occurs. In n-type binary semiconductors, this gives rise to two LO phonon–plasmon coupled modes (LOPCMs) which are denoted by L_+ and L_- [1]. The L_+ mode shows phonon-like character for low carrier density and plasmon-like character for high carrier concentration, while for the L_- mode these characters are reversed. In the intermediate frequency range, the coupled modes have a mixed character. In a ternary alloy with two-mode behaviour there are three coupled modes as a consequence of the existence of separate LO modes associated with each of the two sublattices [2–5]. The highest frequency mode (L_+) presents a behaviour similar to its binary system counterpart, displaying a rapid upward frequency shift with increasing carrier concentration. The lowest frequency coupled mode (LFCM) is analogous to the L_- mode of binary compounds, being plasmon-like for low carrier densities and becoming phonon-like for high carrier densities, when its frequency asymptotically approaches the lower TO mode frequency. A third coupled mode, the intermediate frequency coupled mode (IFCM), occurs

in the gap between the optical frequencies of the two sublattices. This mode is phonon-like except in the vicinity of the plasma frequency and is labelled as L_0 by some authors [2, 3, 5].

The carrier density dependence of LOPCMs in n-$In_{0.53}Ga_{0.47}As$ has been recently reported [4], and it has been found to differ significantly from the typical behaviour that is well established for other alloys. In contrast with other III–V alloys such as $Al_xGa_{1-x}As$, where all LOPCM branches exhibit a frequency increase with increasing free electron density [2], only the L_+ branch shows such trend in n-$In_{0.53}Ga_{0.47}As$ whereas the two lower-frequency branches (IFCM, LFCM) decrease in frequency as the carrier density increases. It should be noted that in the case of $In_{0.53}Ga_{0.47}As$ the frequencies of the two lower-frequency coupled modes lie well within the single-particle excitation region, where intraband single-electron transitions remove energy from the collective coupled mode and, as a result, the LF and IFCMs become heavily damped. Both heavily damped modes display only a small dispersion with electron density and their respective frequencies asymptotically approach the TO frequencies of each of the two sublattices [4].

Raman scattering is a unique tool to study dispersion effects on the frequencies of the coupled modes in polar semiconductors, since the magnitude of the wavevector q involved in the scattering process is large enough and can be readily varied by changing the excitation wavelength. LOPCM wavevector dispersion has been studied by means of Raman scattering in GaAs [1, 6–8] and InP [9], where a continuous upward shift of the L_+ frequency is observed for increasingly shorter excitation wavelengths.

To our knowledge, no study of wavevector dispersion of LOPCMs on ternary alloys has been published so far. In this paper we present a Raman scattering study of the plasmon wavevector dependence in the $In_{0.53}Ga_{0.47}As$ alloy lattice-matched to InP. The frequencies of the heavily damped LF and IFCMs show very little variation with the excitation wavevector, whereas for high carrier concentrations the L_+ mode is plasmon-like and its frequency is well above the single-particle excitation region. Consequently, owing to the small electron effective mass of $In_{0.53}Ga_{0.47}As$, the L_+ mode exhibits a strong wavevector dependence and we focus on this mode to carry out our study of LOPCM wavevector dependence in the $In_{0.53}Ga_{0.47}As$ alloy.

In contrast with the typical LOPCM dependence on excitation wavelength previously reported for GaAs and InP, the Raman peak associated with the L_+ mode exhibits an upward frequency shift for decreasing excitation wavelengths down to 488 nm and then shifts downwards and becomes notoriously broadened for shorter excitation wavelengths. This is well accounted for by calculations based on the Lindhard–Mermin model, which show that the variation of the optical constants of $In_{0.53}Ga_{0.47}As$ close to the E_1 and $E_1 + \Delta_1$ resonances play an important role in the anomalous behaviour of the L_+ mode.

2. Experiment

An n-type, Si-doped $In_{0.53}Ga_{0.47}As$ layer was grown by molecular beam epitaxy on semi-insulating (Fe-doped) (001)-oriented InP substrate. The free electron concentration in the layer, as determined from a line-shape fit to the L_+ Raman peak [4], was 5.4×10^{18} cm^{-3}. The doping level of the sample was selected so as to produce a high-mobility plasma that yielded a well-defined plasmon-like L_+ mode well away from the single particle excitation regime for all the wavevectors studied.

The Raman measurements were carried out at room temperature on a (001) face in $z(xy)\bar{z}$ backscattering configuration. The Raman spectra were excited with the 528.7, 514.5, 501.7, 488.0, 476.5, and 457.9 nm lines of an Ar^+ laser, as well as with 720 and 700 nm excitation wavelengths using a Ti–sapphire laser. For shorter excitation wavelengths the absorption is

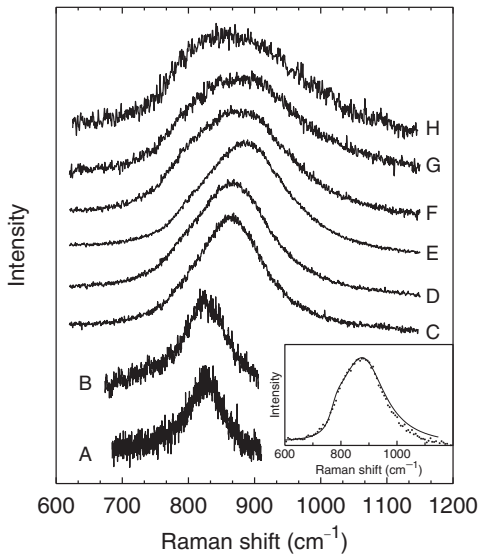

Figure 1. Raman spectra of the L_+ mode of an n-$In_{0.53}Ga_{0.47}As$ sample with $N_e = 5.4 \times 10^{18}$ cm^{-3} obtained using different excitation wavelengths. The spectra were taken at room temperature in the $z(xy)\bar{z}$ backscattering configuration. The excitation wavelengths were 720 (A), 700 (B), 528.7 (C), 514.5 (D), 501.7 (E), 488.0 (F), 476.5 (G), and 457.9 nm (H). Inset: a comparison of the calculated L_+ lineshape (solid curve) with the experimental Raman spectrum (dots) for the 488 nm excitation. The theoretical curve was calculated using the Lindhard–Mermin model for $N_e = 5.4 \times 10^{18}$ cm^{-3} and $\Gamma_e = 50$ cm^{-1} taking into account absorption effects.

very high and the light only probes a superficial region mainly within the depletion zone, whereas for longer excitation wavelengths the signal is extremely weak due to the low Raman scattering efficiency of $In_{0.53}Ga_{0.47}As$ in the near-infrared spectral region. The laser power on the samples was kept at $\approx$75 mW. The Raman spectra were recorded using a Jobin Yvon T64000 spectrometer equipped with a charge coupled device detector cooled with liquid nitrogen, with 100 μm slits. To take into account possible compositional fluctuation of the alloy across the wafer [10], Raman spectra were recorded at four different points of the sample for each laser line to obtain an average L_+ frequency and an estimation of the frequency fluctuation.

3. Results and discussion

Figure 1 shows the room temperature Raman spectra of the L_+ mode of an n-$In_{0.53}Ga_{0.47}As$ sample with $N_e = 5.4 \times 10^{18}$ cm^{-3} for the range of excitation wavelengths used. The electron density in this sample is high enough to ensure that the L_+ mode is well away from the single-particle excitation regime [4] and therefore the L_+ mode excited in the Raman experiments exhibits a clear plasmon-like character. The intensity of the L_+ Raman peak displays variations for the different excitation lines and the spectra shown in figure 1 have been normalized for convenience. Raman scattering efficiency of $In_{0.53}Ga_{0.47}As$ dramatically falls for excitation wavelengths in the red and near-infrared spectral region, and hence a lower signal-to-noise ratio is apparent in spectra A and B of figure 1. As can be seen from figure 1, the L_+ Raman peak shifts to higher frequencies and broadens notably as the excitation wavelength is reduced from 720 nm (A) down to 501.7 nm (E). For shorter excitation wavelengths (F–H), the broadening of the L_+ Raman peak is even more pronounced, but it shows a clear downward frequency shift.

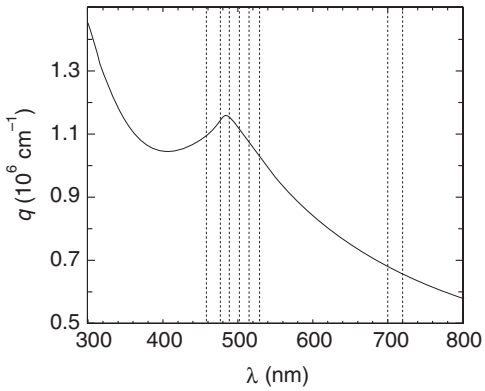

Figure 2. The wavevector transferred in backscattering geometry as a function of excitation wavelength, as calculated for $In_{0.53}Ga_{0.47}As$ from ellipsometry data taken from [11]. The dotted lines indicate the wavelengths used in our Raman measurements.

Table 1. Parameters of $In_{0.53}Ga_{0.47}As$ at room temperature which are used for the q-dispersion calculation of the L_+ mode.

Symbol	Description	Value (cm^{-1})	Reference
$\omega^0_{LO,A}$	LO InAs mode	238	Present work[a]
$\omega^0_{LO,B}$	LO GaAs mode	291	Present work[a]
$\omega^0_{TO,A}$	TO InAs mode	216	Present work[a]
$\omega^0_{TO,B}$	TO GaAs mode	267	Present work[a]
Γ_A	Damping constant of InAs phonon	16	Present work[a]
Γ_B	Damping constant of GaAs phonon	7	Present work[a]
$\omega_{LO,A}$	Alloy InAs-like LO mode	233	Present work[a]
$\omega_{LO,B}$	Alloy GaAs-like LO mode	270	Present work[a]
$\omega_{TO,A}$	Alloy InAs-like TO mode	226	[13]
$\omega_{TO,B}$	Alloy GaAs-like TO mode	254	[13]

[a] Experimentally determined from Raman spectra at 300 K.

To understand the changes observed in the L_+ Raman peak for the different excitation wavelengths used we have to consider the variation of the optical coefficients of $In_{0.53}Ga_{0.47}As$ over the visible range of the spectrum, which includes the E_1 and $E_1 + \Delta_1$ gaps, reported at 2.570 and 2.829 eV, respectively, at room temperature [11]. The broadening of the L_+ peak for increasingly shorter wavelengths is due to the increase of optical absorption near the E_1 and $E_1 + \Delta_1$ gaps [11], which yields a large uncertainty in the wavevector involved in the Raman scattering process [12]. Therefore, it is clear that the energy dependence of the optical properties of $In_{0.53}Ga_{0.47}As$ in the vicinity of the E_1 and $E_1 + \Delta_1$ gaps plays an important role in the observed coupled-mode behaviour.

Kelso *et al* [11] reported the real and imaginary parts n and k of the complex index of refraction of $In_{0.53}Ga_{0.47}As$, derived from the pseudodielectric function they obtained from ellipsometry measurements. In their data, a local maximum of the real part of the index of refraction n can be observed close to the E_1 transition, whereas a steep increase of the extinction coefficient k occurs between the E_1 and $E_1 + \Delta_1$ critical points. From these data, we have calculated the Raman scattering wavevector transferred in backscattering geometry $q = 4\pi n/\lambda$ for a given excitation wavelength λ. In figure 2 we plot the LOPCM wavevector as a function of excitation wavelength. We note that, as a result of the maximum of n around

the E_1 critical point, the LOPCM wavevector excited in Raman measurements displays a local maximum in the visible wavelength range. This implies that there is an upper limit to the q-values which are accessible using the visible lines of the Ar^+ laser. Whereas the LOPCM wavevector increases with decreasing excitation wavelength, for excitation lines shorter than the 488 nm line the LOPCM wavevector decreases again, thus precluding the investigation of coupled mode dispersion for $q \gtrsim 1.16 \times 10^6\ \mathrm{cm}^{-1}$. This upper limit to the accessible q-values for visible excitation wavelengths together with the large variation of the absorption coefficient in the vicinity of the E_1 and $E_1 + \Delta_1$ critical points explain the frequency downshift of the L_+ Raman peaks observed for the shorter excitation wavelengths.

In order to perform a quantitative analysis of the L_+ mode dispersion in $In_{0.53}Ga_{0.47}As$ observed in our experiments, we have applied a Lindhard–Mermin model [4] to calculate the L_+ frequency for the range of excitation wavelengths used. In this model, the dielectric response of the free electrons is evaluated using the Lindhard–Mermin prescription

$$\chi_e(q, \omega + i\Gamma_e) = \frac{(1 + i\Gamma_e/\omega)\chi_e^L(q, \omega + i\Gamma_e)}{1 + i\Gamma_e \chi_e^L(q, \omega + i\Gamma_e)/(\omega \chi_e^L(q, 0))}, \tag{1}$$

where Γ_e is a phenomenological electronic damping constant and $\chi_e^L(q, \omega)$ is given by the Lindhard integral

$$\chi_e^L(q, \omega) = \frac{e^2}{2\pi^3 q^2} \int f(E_F, T, k) \frac{E(q + k) - E(k)}{[E(q + k) - E(k)]^2 - (\hbar\omega)^2}\, d^3k. \tag{2}$$

Here $f(E_F, T, k)$ is the Fermi–Dirac distribution function and $E(q)$ is the conduction band dispersion. Equation (2), which is derived from quantum-mechanical first-order perturbation theory, contains explicitly the q-dependence of the electronic susceptibility and is expected to provide a good description of the wavevector dependence of the coupled modes.

In polar lattices the collective excitations of the free charge couple to the longitudinal optical modes. For the case of a ternary alloy, $A_xB_{1-x}C$, two systems of oscillators exist corresponding to the two sublattices. They are coupled via the macroscopic electric field giving rise to a mean dielectric function of the alloy that can be expressed as [4]

$$\varepsilon(\omega, x) = \varepsilon_\infty(x) + 4\pi \sum_{i=A,B} \chi_i(\omega, x) + 4\pi \chi_e(\omega), \tag{3}$$

where

$$\chi_i(\omega, x) = x_i \frac{\epsilon_{\infty,i}}{4\pi} \frac{(\omega_{LO,i}^0)^2 - (\omega_{TO,i}^0)^2}{\omega_{TO,i}^2 - \omega^2 - i\Gamma_i\omega} \tag{4}$$

is the i-sublattice contribution to the susceptibility, with a phenomenological damping constant Γ_i. In equation (4), $\omega_{LO,i}^0$ and $\omega_{TO,i}^0$ ($i = A, B$) are the LO and TO phonon frequencies of the pure end-member compounds, whereas $\omega_{TO,i}$ is the TO phonon frequency of the alloy i sublattice. The Raman scattering cross section, which is proportional to $\mathrm{Im}\{[-1/\epsilon(\omega, x)](1 + \Xi)\}$, was calculated using the Hon–Faust formalism [4]. For ternary alloys, Ξ contains corrections associated with each sublattice, proportional to $\chi_i(\omega, x)$, and interference cross terms proportional to $\chi_A(\omega, x)\chi_B(\omega, x)$. The main effect of coupling with free charge is reflected in the Raman cross section through an additive contribution $4\pi\chi_e(\omega)$ to the effective dielectric function (see equation (3)). The presence of free charge also gives rise to additional interference cross terms proportional to $\chi_e(\omega)\chi_i(\omega, x)$ in the scattering cross section [4]. We list in table 1 the relevant parameters of the model used for the q-dispersion calculation at room temperature.

Figure 3 shows the results of the theoretical q-dispersion calculation compared with the experimental points obtained from the Raman measurements. The dashed–dotted curve

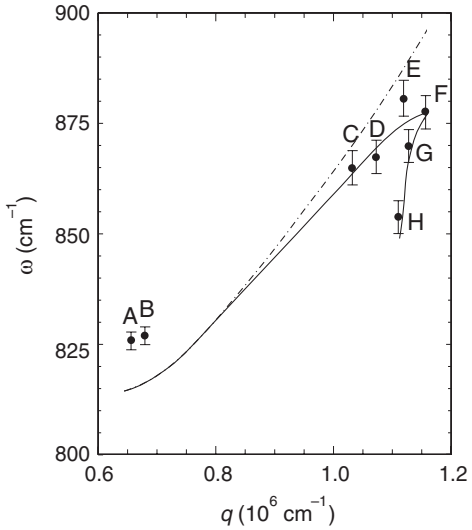

Figure 3. Wavevector dispersion of the L_+ mode for n-$In_{0.53}Ga_{0.47}As$ with a free electron density of 5.4×10^{18} cm^{-3} in the wavevector range accessible to Raman scattering measurements. The dashed–dotted line was calculated using the Lindhard–Mermin model neglecting absorption effects. When optical absorption is included in the calculations the solid line is obtained. We also plot the experimental L_+ frequencies obtained from the Raman measurements performed with different excitation lines.

displays the results of the model when absorption effects are neglected. Then, the frequency of the L_+ mode steadily increases with increasing wavevector. As already mentioned, only q-values up to $q_{\max} \approx 1.16 \times 10^6$ cm^{-1} are accessible by means of Raman measurements by reducing the excitation wavelength. Shorter wavelengths probe wavevectors smaller than $q_{\max}$ and the theoretical curve folds back on itself. Whereas the experimental points A to E follow the trend of increasing frequency predicted by the calculation, points F to H clearly deviate from the behaviour expected when absorption is neglected.

The downward frequency shift of the L_+ peak observed for the shortest excitation wavelengths can be attributed to the strong optical absorption of $In_{0.53}Ga_{0.47}As$ for the blue lines of the Ar^+ laser. Next, we support this point by calculating the L_+ dispersion taking into account the optical absorption effects.

In opaque materials, the spatial variation of the optical fields gives rise to a range of wavevectors transferred in the Raman scattering process that is determined by the Fourier transforms of the spatially varying fields. The wavevector distribution transferred in backscattering configuration is given by [12]

$$\mathcal{L}(q) = \frac{\alpha}{\pi[(q_0 - q)^2 + \alpha^2]}, \tag{5}$$

where α is the absorption coefficient and the central q-value of the transferred wavevector distribution is given by $q_0 = 4\pi n/\lambda$, λ being the excitation wavelength. We have included the absorption effects in our model by calculating the L_+ Raman peak as the weighted average of L_+ lineshapes over the wavevector distribution $\mathcal{L}(q)$ given by equation (5). The solid curve in figure 3 shows the L_+ Raman mode dispersion obtained from this calculation. For small wavevectors, i.e. small excitation energy, the curves with and without absorption effects are practically coincident. However, as the excitation energy approaches the E_1 and $E_1+\Delta_1$ critical points the steep increase of the absorption coefficient produces a sizable downward shift of

the L_+ Raman peak. The cusp of the dispersion curve (solid curve of figure 3) corresponds to the local maximum of the real part of the index of refraction n, which results in a local maximum of the transferred wavevector as illustrated in figure 2, and roughly coincides with the 488 nm excitation (F). For higher excitation energies, the corresponding wavevectors decrease, retracing the previous q_0-values, while the absorption coefficient keeps increasing. For a given q_0-value in this range two possible excitation lines exist, and the L_+ Raman peak excited with the shortest one shows a higher downward shift due to the increased absorption. This results in a frequency difference in the L_+ Raman peaks corresponding to the duplicated q_0-values that gives rise to a backwards evolving branch in the L_+ Raman peak dispersion. As can be seen in figure 3, the behaviour predicted by the LOPCM model including absorption effects is in good agreement with the Raman measurements carried out at different excitation wavelengths, which showed a marked broadening and frequency downshift for the shortest wavelengths (G and H).

4. Conclusions

We have used Raman scattering to study the wavevector dispersion of the L_+ plasmon–LO-phonon coupled mode in n-$In_{0.53}Ga_{0.47}As$. Because of the proximity of the E_1 and $E_1 + \Delta_1$ critical points, the optical properties of $In_{0.53}Ga_{0.47}As$ exhibit characteristic features in the range of excitation energies used that strongly affect the L_+ Raman peak. On the one hand, the refractive index displays a local maximum in the vicinity of the E_1 transition, and this effectively sets an upper limit to the wavevectors accessible to Raman scattering measurements in the visible excitation range. On the other hand, the steep increase of the optical absorption as the E_1 and $E_1 + \Delta_1$ critical points are approached makes absorption effects very important in Raman spectra excited with the blue lines of the Ar^+ laser. The coupled-mode dispersion in $In_{0.53}Ga_{0.47}As$ for the shorter excitation lines differs significantly from the well-known behaviour for GaAs and InP. The L_+ Raman peak broadens and shows a marked frequency decrease for excitation wavelengths shorter than 488 nm. This behaviour can be explained by taking into account the variation of the optical constants of $In_{0.53}Ga_{0.47}As$ in the range of excitation energies used. Our work shows that, for a given range of excitation wavevectors, the L_+ frequency observed in Raman experiments is not completely determined by the excitation wavevector but it also depends on the excitation wavelength used. This is supported by a calculation of LOPCM dispersion using the Lindhard–Mermin model which nicely reproduces the observed behaviour when absorption effects are included.

Acknowledgments

This work was supported by the Spanish Ministry of Science and Technology. One of us (SH) acknowledges support from Department d'Universitats i Recerca de la Generalitat de Catalunya.

References

[1] Abstreiter G, Cardona M and Pinczuk A 1984 *Light Scattering in Solids IV* vol 54, ed M Cardona and G Güntherodt (Berlin: Springer)
[2] Yuasa T, Naritsuke S, Mannoh M, Shjinozaki K, Yamanaka K, Nomura Y, Mihara M and Ishii M 1986 *Phys. Rev.* B **33** 1222
[3] Maslar J E, Dorsten J F, Bohn P H, Agarwala S, Adesida I, Canau C and Bhat R 1994 *Phys. Rev.* B **50** 17143
[4] Cuscó R, Artús L, Hernández S, Ibáñez J and Hopkinson M 2002 *Phys. Rev.* B **65** 035210

[5] Groenen J, Carles R, Landa G, Guerret-Piécourt C, Fontaine C and Gendry M 1998 *Phys. Rev.* B **58** 10452
[6] Nowak U, Richter W and Sachs G 1981 *Phys. Status Solidi* b **108** 131
[7] Pinczuk A, Abstreiter G, Trommer R and Cardona M 1977 *Solid State Commun.* **21** 959
[8] Abstreiter G, Trommer R, Cardona M and Pinczuk A 1979 *Solid State Commun.* **30** 703
[9] Richter W, Nowak U, Jürgensen H and Rössler U 1988 *Solid State Commun.* **67** 199
[10] Mikkelsen J C Jr and Boyce J B 1983 *Phys. Rev.* B **28** 7130
[11] Kelso S M, Aspnes D E, Pollack M A and Nahory R E 1982 *Phys. Rev.* B **26** 6669
[12] Dresselhaus G and Pine A S 1975 *Solid State Commun.* **16** 1001
[13] Estrera J P, Stevens P D, Glosser R, Duncan W M, Kao Y C, Liuand H Y and Beam E A III 1992 *Appl. Phys. Lett.* **61** 1927